Multiscale fusion of digital rock images based on deep generative adversarial networks

Mingliang Liu[1] and **Tapan Mukerji**[1]

[1] Department of Energy Resources Engineering, Stanford University, USA.

Corresponding author: Mingliang Liu (mliu9@stanford.edu)

Key Points:

- Style-based generative adversarial network (GAN) is effective for augmenting sparse high-resolution SEM images.
- Cycle-consistent GAN is successfully applied to integrate unpaired multi-resolution digital rock images.
- The method shows promise in the reconstruction of high-resolution digital rocks that accurately capture micro-structures at multi-scales.

ABSTRACT

Computation of petrophysical properties on digital rock images is becoming important in geoscience. However, it is usually complicated for natural heterogeneous porous media due to the presence of multiscale pore structures. To capture the heterogeneity of rocks, we develop a method based on deep generative adversarial networks to assimilate multiscale imaging data for the generation of synthetic high-resolution digital rocks having a large field of view. The reconstructed images not only honor the geometric structures of 3-D micro-CT images but also recover fine details existing at the scale of 2-D scanning electron microscopy images. Furthermore, the consistency between the real and synthetically generated images in terms of porosity, specific surface area, two-point correlation and effective permeability reveals the validity of our proposed method. It provides an effective way to fuse multiscale digital rock images for better characterization of heterogeneous porous media and better prediction of pore-scale flow and petrophysical properties.

Plain Language Summary

Digital rock physics is an effective approach to characterize pore microstructures and predict effective physical properties of porous medium. However, there is an inherent trade-off between imaging resolution and field of view (FoV) due to the limitations of different imaging techniques: high-resolution data can resolve pore structures up to nano scale but the FoV is not large enough to capture a representative volume element; low-resolution data have larger FoV but cannot capture the fine features. To overcome the trade-off, it is necessary to develop a workflow of multiscale data fusion for the reconstruction of digital rocks with both high-resolution and large FoV. The major challenges are (1) that the high-resolution images are usually limited in number and (2) that the imaging data are typically acquired at different locations of the rock sample, which means that the training samples are unpaired. To address such challenges, we use a

style-based generative adversarial network (GAN) to augment the limited high-resolution data and then use a cycle-consistent GAN to integrate the unpaired digital rock data from multiple sources. The proposed method performs well at reconstructing high-resolution rock models that allows more accurate fluid flow simulation at pore-scale and prediction of effective properties.

1. Introduction

Having a deep understanding of pore-scale processes in porous media is of critical importance for various subsurface applications, such as water resources, oil and gas recovery and carbon dioxide sequestration. The conventional method that takes the physical experiments on core plugs are typically time-consuming and limited by the lab environment. As an alternative approach, digital rock physics (DRP) performs numerical simulations of pore-scale processes of interest directly on digital scans of porous rocks (Keehm et al., 2001 and 2004; Andrä et al., 2013a and 2013b; Blunt et al., 2013; Saxena et al., 2017). It provides a non-destructive means of repeatedly carrying out numerical simulations under different scenarios on the same rock sample. The simulations at pore-scale can then be interpretated to derive macroscopic reservoir properties (e.g., permeability, formation factor, elastic moduli, etc.) and used for sensitivity analysis. A representative elementary volume (REV) of the rock sample with high resolution is an important prerequisite for accurate digital rock physics results. However, in practice, there is an inherent trade-off between field of view (FoV) and image resolution due to the limitation of imaging techniques (Wildenschild et al., 2002; Wildenschild and Sheppard, 2013). Low-resolution imaging cannot resolve micro pores, which often makes the estimated rock properties to be underestimated or overestimated with regards to experimental measurements. On the other hand, the high-resolution image may not capture a REV due to the small FoV.

One way to overcome the trade-off is to integrate imaging data from multiple sources, such as 3-D micro-CT images at the micron scale and 2-D SEM images at the nano scale. Traditional solutions to this challenging problem are mainly stochastic methods based on the spatial statistical information (e.g., two-point correlation functions and multiple-point statistics). Jiao et al. (2007) modeled heterogeneous materials from two-point correlation functions using simulated annealing. Okabe and Blunt (2007) reconstructed 3-D pore space structure by integrating micro-CT images at the micron-scale that resolve large pores with statistically simulated high-resolution images from 2-D thin sections that provides finer-scale features. Mohebi et al. (2009) proposed a statistical method to fuse low-resolution measurements with a high-resolution prior model. Tahmasebi et al. (2015) proposed a multiscale and multiresolution reconstruction method to generate 3-D models of shales using 2-D images.

In recent years, deep learning methods have been developed to alleviate the trade-off between resolution and FoV. Wang et al. (2019) and Da Wang et al. (2019) applied convolutional neural networks (CNN) for micro-CT image enhancement. Da Wang et al. (2020) proposed a generative adversarial network

(GAN) to increase the micro-CT image resolution. The above works are based on supervised learning methods that require a large number of paired training data of corresponding low- and high-resolution images. However, in practice, the paired training data are often not available because the sample locations of imaging data are often different. To circumvent this limitation, Niu et al., (2020) proposed a cycle-in-cycle GAN to deal with the unpaired training data for boosting lateral resolution of micro-CT images. You et al. (2021) developed a progressive growing GAN to increase the vertical resolution by combination with the technique of GAN inversion. The deep learning methods are powerful for resolution enhancement of micro-CT images and have high perceptive accuracy compared to traditional interpolation algorithms (e.g., nearest neighborhood and bicubic interpolation). However, previous works mainly focused on the super-resolution problem aiming to increase the resolution of micro-CT images by two or four times. They are useful to make the micro-CT images sharper but cannot resolve pore structures at multiscale or integrate data from different imaging modalities such as micro-CT and SEM images.

The major challenges in multiscale digital rock data fusion are (1) that the high-resolution images are usually limited in number, which would make the model to be easily overfitted and (2) that the digital rock images from multiple sources are typically acquired at different locations of the rock sample, which means that the training samples are unpaired and therefore, supervised methods of machine learning are not applicable. In this letter we propose an innovative method to solve this problem based on deep neural networks. It uses a style-based GAN (Karras et al., 2019; Karras et al., 2020a and 2020b) to augment the limited high-resolution images and then fuses unpaired data at different resolutions by a cycle-consistent GAN (CycleGAN) (Zhu et al., 2017). The disentanglement representation learning of the style-based GAN allows us to generate images with different styles by sampling in different regions of the latent space. With such an advantage, we can train multiple CycleGAN models by feeding training samples with different styles and thus generate multiple high-resolution realizations of the rock that are consistent with the input of low-resolution micro-CT.

1. Methodology and Data

The proposed workflow of multiscale digital rock data fusion is illustrated in Figure 1. In this study, we have five carbonate samples, most of which exhibit high heterogeneity and anisotropy. Each sample has one high-resolution 2-D SEM image with a size of about 7500×4500 pixels and two or three low-resolution 3-D micro-CT volumes with a size of about 600×600×900 voxels. The resolutions of the micro-CT images range from 1.0 to 2.0 m, while the resolutions of all SEM images are 0.1 m. A Style-based GAN is first trained to augment the limited number of SEM images and then a CycleGAN is used to reconstruct high-resolution images from low-resolution micro-CT data.

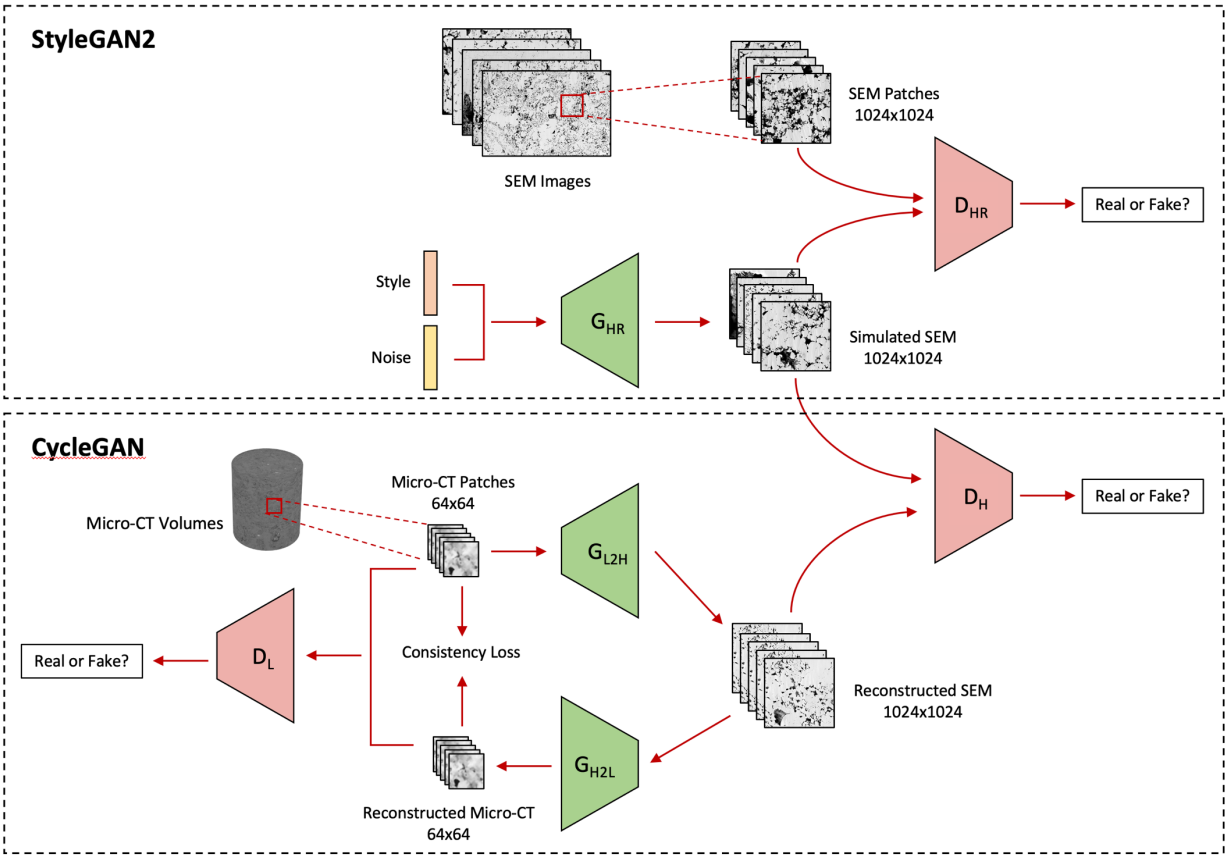

Figure 1. The overall workflow of multiscale digital rock data fusion based on deep generative adversarial networks: G_{HR} is the generator of StyleGAN2 that takes the style latent vector and random noise as input to simulate SEM images; D_{HR} is the discriminator of StyleGAN2 that aims to distinguish between real SEM samples and fake samples generated by G_{HR}; G_{L2H} and G_{H2L} are two generators of CycleGAN that predicts high-resolution image from low-resolution micro-CT data and recovers low-resolution data from high-resolution data, respectively; D_L and D_H are two discriminators corresponding to G_{L2H} and G_{H2L}, respectively.

2.1 SEM Data Augmentation by StyleGAN2-ADA

GANs are a class of generative network models typically consisting of two competing players: a generator network G and a discriminator network D (Goodfellow et al., 2014). The generator G tries to synthesize fake samples $G(z)$ from the input random noise $z \sim p_z(z)$ to fool D by mimicking real samples $x \sim p_{\text{data}}(x)$, while D conversely aims to distinguish between real samples $x \sim p_{\text{data}}(x)$ and fake samples $G(z)$. The notation $y \sim p(y)$ indicates that the random variable y

is distributed according to the probability distribution $p(y)$. The two networks G and D are trained in an adversarial manner, which is equivalent to playing a minimax game with a loss function $\mathcal{L}_{\mathrm{GAN}}(D, G)$ given by

$$\min_G \max_D \mathcal{L}_{\mathrm{GAN}}(D, G) = E_{x\sim p_{\mathrm{data}}(x)} \left[\log D(x)\right] + E_{z\sim p_z(z)} \left[\log\left(1 - D\left(G(z)\right)\right)\right]. \tag{1}$$

With such an adversarial training scheme, GANs have the ability of producing high quality sharp images, outperforming approaches based on pixel-wise mean square error (MSE) loss (Goodfellow et al., 2014).

Karras et al. (2018, 2019) developed StyleGAN and StyleGAN2, two variants of GANs, which are powerful in high-resolution images generation. They can control not only the style (global features) of the image at different scales but also stochastic details (local features). Since StyleGANs are unsupervised, they are well-suited for datasets without conditional labels, which are often common in real applications. To address the long-standing challenge in GANs of training with small dataset, (in which case the discriminator will quickly be overfit to the training samples resulting in divergence of the training), Karras et al. (2020) improved StyleGAN2 by introducing an adaptive discriminator augmentation (ADA) mechanism, which is called StyleGAN2-ADA. With such an augmentation mechanism, the style-based GANs perform well with several thousand or even only several hundred training samples. A detailed description of ADA can be found in the Supporting Information S1.

StyleGAN2 consist of two components: a mapping network and a synthesis network. The goal of the mapping network is to encode the input random noise $\mathbf{z} \in \mathbb{Z}$ into a set of intermediate vectors $\mathbf{w} \in \mathbb{W}$ using fully connected layers. Each intermediate vector $\mathbf{w}$ is further transformed to produce a style scalar s by an affine transformation $\mathbf{A}$. The major benefit of the mapping network is that it is helpful to disentangle the latent representation and therefore makes our model easier to be interpreted. Then, the synthesis network incorporates the styles s via a weight demodulation operation to generate the artificial images starting from low resolution (4×4) and continuing to higher resolution (8×8, 16×16, ..., 1024×1024) by convolutional layers. The shallower the layer in which the style s is incorporated, the coarser the level of details is affected. For example, the first few styles affect the coarse level of details (4×4), while the last few styles affect the fine level of details (1024×1024). This architecture enables the StyleGAN2 to control the global features of images at different scales. To control stochastic variations of generated images at different levels of details, random noise after another affine transformation $\mathbf{B}$ is injected to the feature maps of the convolutional blocks. It allows the generator to only change the local features, leaving the overall styles and high-level details intact. A detailed network architecture of StyleGAN2 can be found in the Supporting Information Figure S2.

2.2 Multiscale Digital Rock Images Fusion by CycleGAN

Another challenge in fusing multiscale digital rock images is that the images are acquired at different locations of the rock sample, which means that the training samples are unpaired. For this reason, we adopt a CycleGAN, which is an unsupervised method designed for image cross-domain transfer (Zhu et al., 2017). Specifically, in this study, we aim to transfer the micro-CT images from the low-resolution domain LR to the high-resolution domain HR by integrating the information from SEM data.

CycleGAN consists of four networks: (1) a generator G_{L2H} mapping the images from domain LR to domain HR, (2) a generator G_{H2L} mapping the images from domain HR to domain LR, (3) a discriminator D_H aiming to encourage G_{L2H} to transfer LR into outputs indistinguishable from domain HR and (4) a similar discriminator D_L for G_{H2L}. The major difference of CycleGAN from traditional GANs is that it includes two generators to constrain each other. It ensures that G_{L2H} outputs the high-resolution image that is conditional to the input low-resolution image and vice versa for G_{H2L}. To achieve this goal, apart from the adversarial loss (Eq. 1), we need to add a regularization term to the loss function of the generators, namely the cycle-consistent loss given by

$$\mathcal{L}_{\mathrm{CYC}}\left(G_{L2H},\ G_{H2L}\right) = E_{x\sim p_{\mathrm{LR}}(x)}\left[\left\|G_{H2L}\left(G_{L2H}(x)\right)\ - x\right\|_1\right] + E_{y\sim p_{\mathrm{HR}}(y)}\left[\left\|G_{L2H}\left(G_{H2L}(y)\right)\ - y\right\|_1\right] \quad (2).$$

The first term in Eq. 2 aims that for each image x from domain LR, the image transfer cycle can transform x back to the original input, i.e., $G_{H2L}\left(G_{L2H}(x)\right) \approx x$. Similarly, for each image y from domain HR, the second term in Eq. 2 ensures backward cycle consistency: $G_{L2H}\left(G_{H2L}(y)\right) \approx y$. A detailed network architecture of CycleGAN can be found in the Supporting Information Figure S3.

2.3 Data Preparation and Training

The training samples consist of two datasets: (1) low-resolution sub-images of micro-CT with a size of 64×64 and (2) high-resolution sub-images of SEM with a size of 1024×1024. Considering that there are only a limited number of real SEM images, we extract the high-resolution sub-images with a 70% overlap between sequential sub-images (with a sliding stride of 500 pixels) to increase the number of training samples. In total, there are 371 high-resolution samples of SEM. The micro-CT data are sufficient in number, so we randomly extract the low-resolution sub-images without any overlap. In total, there are 200,000 low-resolution samples of micro-CT images.

The training of the networks includes two steps. We start with the StyleGAN2-ADA training for SEM data augmentation. It aims to learn the underlying probability distribution (or manifold) where the real SEM sub-images lie. The StyleGAN2-ADA is trained in parallel with four Nvidia A100 GPUs each with 40 GB memory. It takes approximately 24 hours to converge. After training, we use the generator of the StyleGAN2-ADA to simulate 200,000 high-resolution sub-images to keep the number comparable with the low-resolution images. Such data augmentation would be helpful for the training of the following CycleGAN to avoid overfitting. After training the CycleGAN, we can use the generator

G_{LH} to transfer the low-resolution images with a size of 64×64 to the high-resolution domain with a size of 1024×1024. The training of CycleGAN takes approximately 24 hours with one Nvidia A100 GPU.

1. **Results**

Figures 2a and 2b show the high-resolution images extracted from the real SEM data and those simulated by the trained StyleGAN2-ADA with different global styles but constant noise as input, respectively. The simulated images capture the fine details of microstructures in the SEM data and are visually indistinguishable from the real samples. Moreover, most pore types, i.e., inter- and intra-granular pore and microfracture from the nano to micron scale, are accurately recovered. It indicates that undesirable mode collapse does not occur in the training and the trained StyleGAN2-ADA can guarantee the diversity of image generation. To quantitively evaluate the quality of the generated images, we compute the porosity, specific surface area and two-point correlation of both the real and simulated images. As shown in Figure 3, the distributions of the synthetic and real samples are consistent. It also indicates that the microstructural details of the SEM data are well captured by the StyleGAN2-ADA. The correlation curves shown in Figure 3c are close to the exponential model defined as $R(h) = e^{-h/\lambda}$ where h is the lag distance and λ is the correlation length. The correlation length λ of each sample in Figure 3d is obtained by fitting the exponential model $R(h)$ to the two-point correlation curve. As can be seen from the histograms of correlation lengths, the synthetic samples, while broadly consistent with the true samples, do tend to have slightly longer correlation lengths, indicating that some of the generated synthetic samples may be smoother than the true images. Figure S4 in the Supporting Information shows the synthetic images generated with fixed styles but different noise. The generated samples look similar in global features but different in local features and they are very close in terms of the porosity, specific surface area and two-point correlation (Figure S5 in the Supporting Information). The above different behaviors with constant and changing global style vectors indicate that the style-based GAN has a good ability of separating the global and local styles underlying the training images. Thanks to the disentangled representation of the latent space, we can generate new images by interpolation in the latent style space. As shown in Figure S6 in the Support Information, the generated images are smoothly transformed from one end-member to another with progressive interpolation between the latent space end-members.

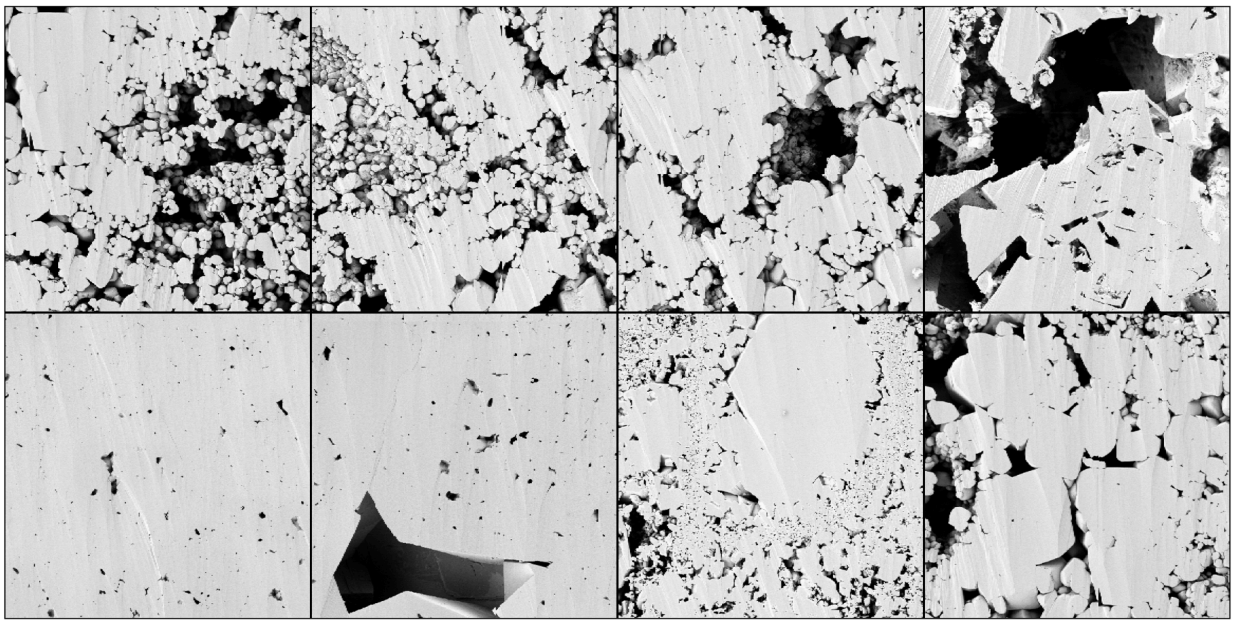

(a)

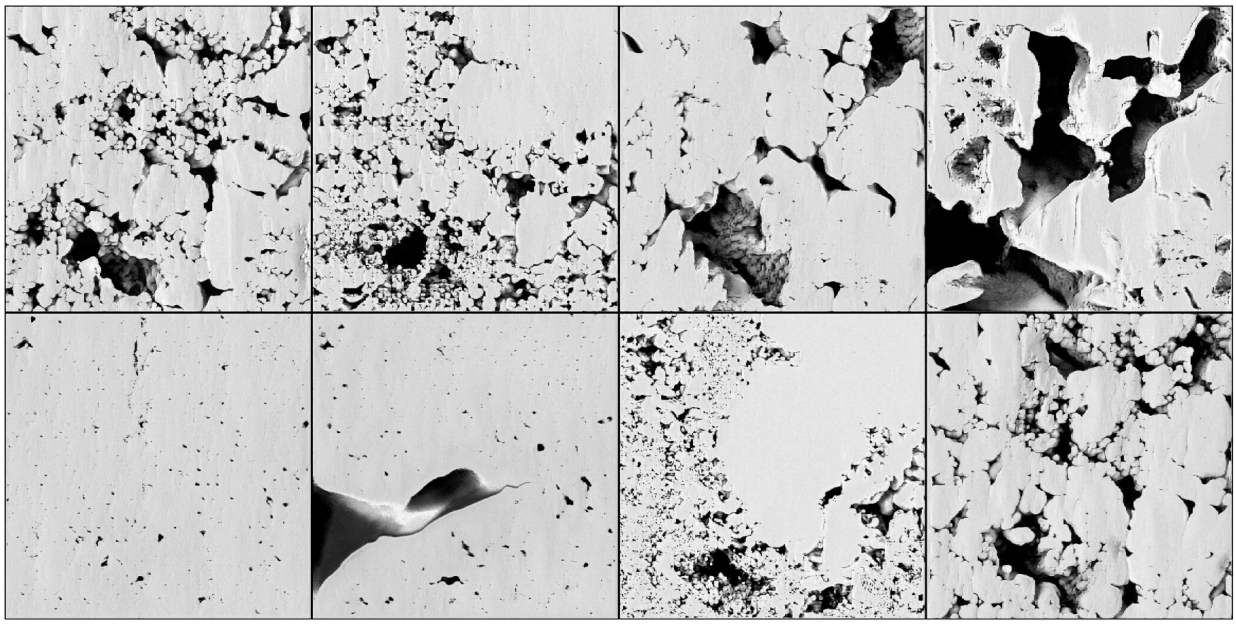

(b)

Figure 2. (a) real SEM images; (b) synthetic images generated by the trained StyleGAN2-ADA with different global styles and constant noise. The image size is 1024×1024 and the resolution is 0.1 m.

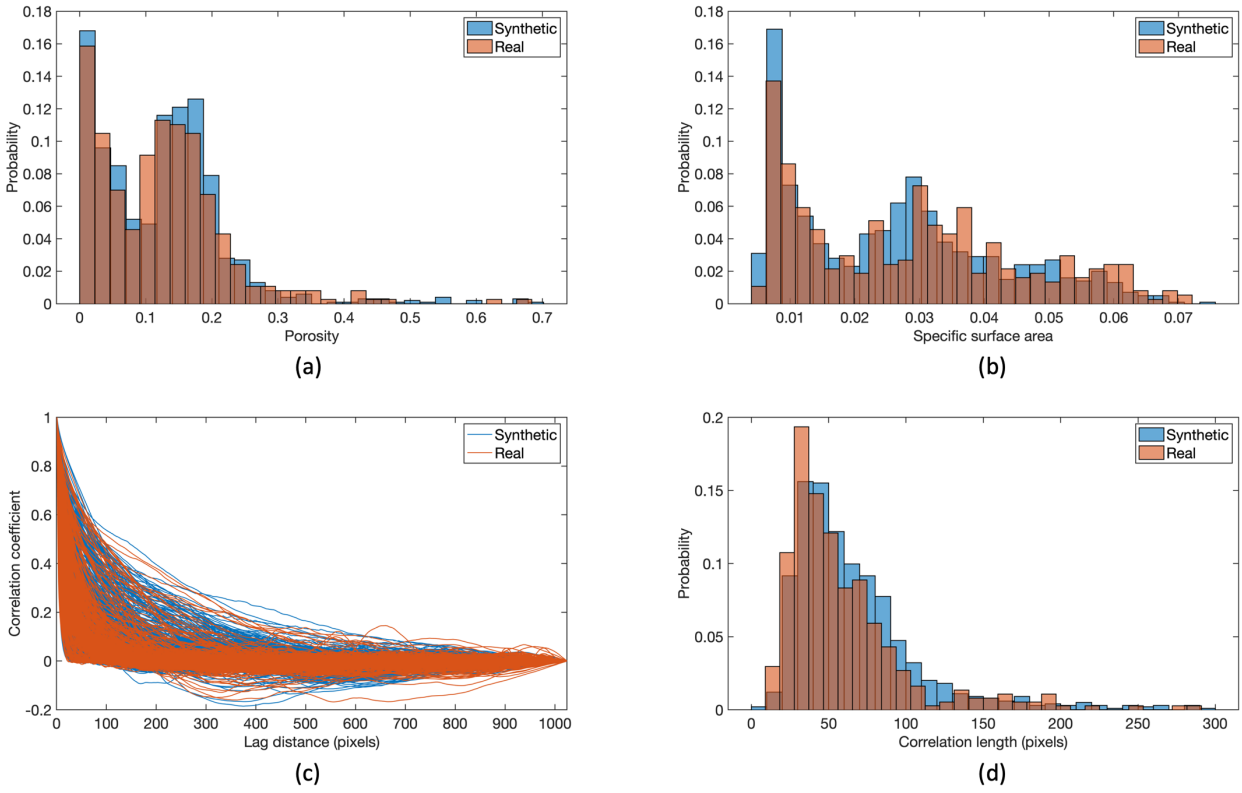

Figure 3. Microstructure analyses for the real and synthetic SEM samples: (a) porosity; (b) specific surface area; (c) two-point correlation function; (d) two-point correlation length.

Figure 4a and 4b shows the predicted high-resolution images from micro-CT data using the trained CycleGAN. With the generator G_{L2H} of the trained CycleGAN, the low-resolution micro-CT image with a size of 64×64 can be increased by 16 times to the high-resolution domain with a size of 1024×1024. We can see that the reconstructed images not only keep the geometric structures of the input micro-CT images but also recover the fine details present in the SEM data. The recovered fine microstructural details would be helpful to accurately predict pore-scale fluid flow and effective petrophysical properties. Thanks to the disentanglement of the latent style space learned by the StyleGAN2, we can control the styles of the synthetic SEM images by sampling in different regions of the latent space. As illustrated in the Supporting Information Figure S7, we can train multiple CycleGAN models by feeding training samples with different styles and thus generate multiple high-resolution realizations of the rock that

all are consistent with the input of low-resolution micro-CT.

Then, we use the CycleGAN to down-scale the entire 3-D micro-CT volumes. The prediction is performed slice by slice and each slice is divided into patches with a size of 64×64. The vertical resolution of micro-CT is first increased by 16 times by bicubic interpolation to make the reconstructed rock models have same resolution along all three directions. To mitigate the artifacts at boundaries, there is an overlap of 8 pixels between patches. One predicted slice with a larger size of 3584×3584 is shown in the Supporting Information Figure S8. The predicted high-resolution images are close to the true SEM image from the same rock sample in terms of porosity, specific surface area and two-point correlation as illustrated in the Supporting Information Figure S9. Figure 4c and 4d show the pore-scale Stokes flow (the slow, incompressible, viscous steady flow) (Allen, 2021) simulated by the LIR solver of the GeoDict software (Linden et al., 2015) over a sub-cube of micro-CT with a size of 64×64×64 and the reconstructed high-resolution rock, respectively. We can observe more details from the reconstructed high-resolution model and thus have deeper understanding of physical procedures at pore-scale. Figure 4f shows one 3-D realization with a size of 1792×1792×2688 from the micro-CT data with a size of 112×112×168 (Figure 4e). More realizations can be found in the Supporting Information Figure S10. As shown in Table 1, the predicted permeabilities of the reconstructed high-resolution models are more consistent with the permeability from the laboratory core measurement than the prediction from micro-CT data.

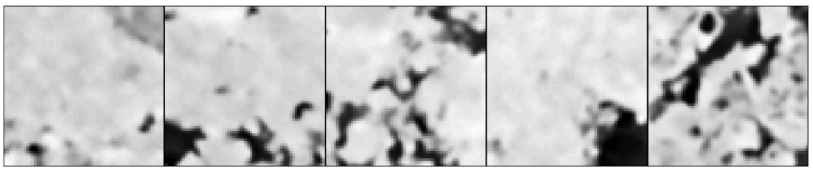

(a)

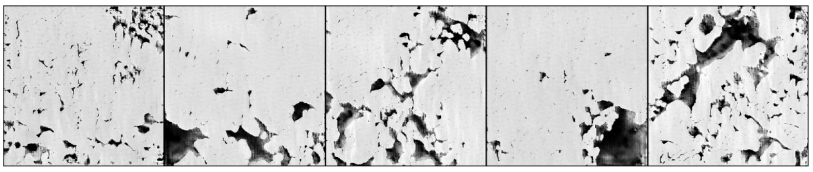

(b)

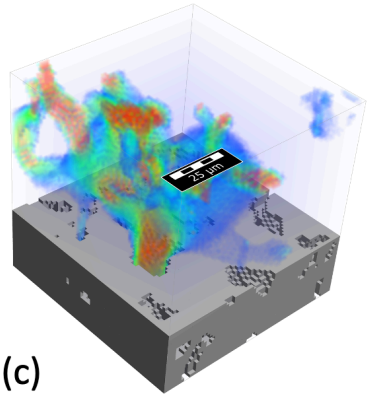

(c)

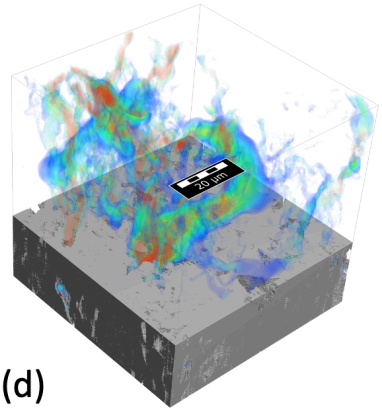

(d)

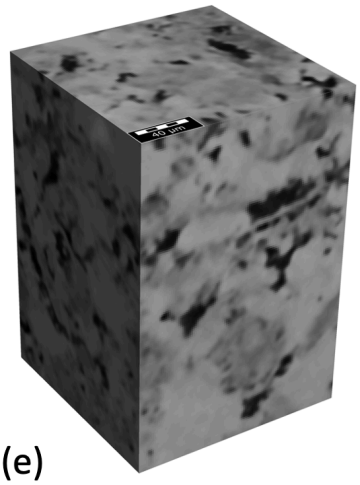

(e)

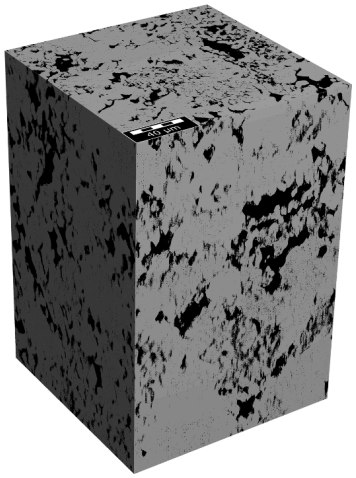

(f)

Figure 4. (a) micro-CT images (64×64; dx=1.6 m) and (b) prediction of CycleGAN (1024×1024; dx=0.1 m); (c) velocity field of fluid flow simulation on the micro-CT sub-cube (64×64); (d) velocity field of the fluid flow simulation on the reconstructed model at the SEM scale (64×64); (e) input micro-CT volume (112×112×168); (f) reconstructed high-resolution model (1792×1792×2688).

Table 1. Porosity and permeability of the low-resolution micro-CT and reconstructed high-resolution realizations (M1-M7) as well as the lab measurement.

	Lab	micro-CT	M1	M2	M3	M4	M5	M6	M7
Porosity	0.19	0.19	0.17	0.16	0.15	0.13	0.23	0.10	0.14
Permeability (mD)	4.0	132.75	1.79	3.98	1.92	4.05	8.70	1.06	2.50

1. Discussion

In recent years, attempts have been made to overcome the trade-off between resolution and FoV for digital rock data using deep learning methods (e.g., CNNs and GANs). However, previous works focused on the super-resolution problem aiming to increase the resolution of micro-CT images by two or four times. They are useful to make the micro-CT images sharper but cannot resolve pore structures at multiscale. Our proposed method provides an effective means to reconstruct rock models that accurately capture multiscale pore structures obtained by different imaging methods (e.g., micro-CT and SEM). Due to the limitation of GPU memory and non-availability of 3-D SEM data, the output high-resolution image is only in 2D and with a size of 1024×1024 and therefore, we need to perform the prediction patch-by-patch by dividing the micro-CT slice into sub-images. The straightforward solution to increase the image size is to use more GPUs, but a more efficient way is to decrease the number of network parameters by model compression (e.g., depthwise separable convolutions, network pruning and knowledge distillation). The potential solution to 3-D simulation is to develop a GAN with the generator in 3-D while the discriminator in 2-D which takes the slices sampled from generated synthetic 3-D images and real SEM data. Those are the research directions that we will investigate in future.

1. Conclusion

We presented an innovative approach for fusion of multiscale digital rock images, i.e., low-resolution micro-CT and high-resolution SEM data, using StyleGAN2-ADA and CycleGAN. The StyleGAN2-ADA network is effective to overcome the issue of overfitting due to limited number of SEM images, while the CycleGAN network allows for leveraging unpaired training samples of micro-CT and SEM, which is a common challenge in practice. The application to a carbonate dataset reveals that the proposed methodology is a valid and powerful approach for integrating multiscale digital rock data. The reconstructed rock models accurately capture the micro-structures from both low-resolution micro-CT and high-resolution SEM images. Moreover, the computed effective permeabilities

are more accurate than the prediction directly from micro-CT data by comparison with the laboratory measurement. We conclude that the proposed method provides an efficient means to reconstruct high-resolution digital rocks with large FoV, which is of great significance for the accurate pore-scale flow simulation and petrophysical properties prediction.

Data Availability Statement

The code is freely available on the GitHub repository (https://github.com/theanswer003/MultiscaleDRPNet).

Acknowledgements

We acknowledge Shell for financial support and for providing the digital rock images. This study has mostly been performed using the Sherlock cluster at Stanford University. We are grateful to Stanford University and the Stanford Research Computing Center for providing computational resources and support in this research. We acknowledge the sponsors of the Stanford Center for Earth Resources Forecasting (SCERF) and support from Prof. Steve Graham, the Dean of the Stanford School of Earth, Energy and Environmental Sciences. The authors also would like to thank Math2Market for providing the GeoDict software.

References

- Allen, M.B., 2021. The Mathematics of Fluid Flow in Porous Media, John Wiley & Sons, Hoboken, NJ.
- Andrä, H., Combaret, N., Dvorkin, J., Glatt, E., Han, J., Kabel, M., Keehm, Y., Krzikalla, F., Lee, M., Madonna, C. and Marsh, M., 2013a. Digital rock physics benchmarks—Part I: Imaging and segmentation. Computers & Geosciences, 50, pp.25-32.
- Andrä, H., Combaret, N., Dvorkin, J., Glatt, E., Han, J., Kabel, M., Keehm, Y., Krzikalla, F., Lee, M., Madonna, C. and Marsh, M., 2013b. Digital rock physics benchmarks—Part II: Computing effective properties. Computers & Geosciences, 50, pp.33-43.
- Blunt, M.J., Bijeljic, B., Dong, H., Gharbi, O., Iglauer, S., Mostaghimi, P., Paluszny, A. and Pentland, C., 2013. Pore-scale imaging and modelling. Advances in Water resources, 51, pp.197-216.
- Da Wang, Y., Armstrong, R.T. and Mostaghimi, P., 2019. Enhancing resolution of digital rock images with super resolution convolutional neural networks. Journal of Petroleum Science and Engineering, 182, p.106261.
- Da Wang, Y., Armstrong, R.T. and Mostaghimi, P., 2020. Boosting resolution and recovering texture of 2D and 3D micro-CT images with deep learning. Water Resources Research, 56(1), p.e2019WR026052.
- Karras, T., Laine, S. and Aila, T., 2019. A style-based generator architecture for generative adversarial networks. In Proceedings of the IEEE/CVF

Conference on Computer Vision and Pattern Recognition (pp. 4401-4410).

- Karras, T., Laine, S., Aittala, M., Hellsten, J., Lehtinen, J. and Aila, T., 2020a. Analyzing and improving the image quality of stylegan. In Proceedings of the IEEE/CVF Conference on Computer Vision and Pattern Recognition (pp. 8110-8119).
- Karras, T., Aittala, M., Hellsten, J., Laine, S., Lehtinen, J. and Aila, T., 2020b. Training generative adversarial networks with limited data. arXiv preprint arXiv:2006.06676.
- Keehm, Y., Mukerji, T. and Nur, A., 2001. Computational rock physics at the pore scale: Transport properties and diagenesis in realistic pore geometries. The Leading Edge, 20(2), pp.180-183.
- Keehm, Y., Mukerji, T. and Nur, A., 2004. Permeability prediction from thin sections: 3D reconstruction and Lattice-Boltzmann flow simulation. Geophysical Research Letters, 31(4).
- Linden, S., Wiegmann, A. and Hagen, H., 2015. The LIR space partitioning system applied to the Stokes equations. Graphical Models, 82, pp.58-66.
- Mohebi, A., Fieguth, P. and Ioannidis, M.A., 2009. Statistical fusion of two-scale images of porous media. Advances in water resources, 32(11), pp.1567-1579.
- Niu, Y., Wang, Y.D., Mostaghimi, P., Swietojanski, P. and Armstrong, R.T., 2020. An innovative application of generative adversarial networks for physically accurate rock images with an unprecedented field of view. Geophysical Research Letters, 47(23), p.e2020GL089029.
- Jiao, Y., Stillinger, F.H. and Torquato, S., 2007. Modeling heterogeneous materials via two-point correlation functions: Basic principles. Physical review E, 76(3), p.031110.
- Okabe, H. and Blunt, M.J., 2007. Pore space reconstruction of vuggy carbonates using microtomography and multiple-point statistics. Water Resources Research, 43(12).
- Saxena, N., Hofmann, R., Alpak, F.O., Berg, S., Dietderich, J., Agarwal, U., Tandon, K., Hunter, S., Freeman, J. and Wilson, O.B., 2017. References and benchmarks for pore-scale flow simulated using micro-CT images of porous media and digital rocks. Advances in Water Resources, 109, pp.211-235.
- Tahmasebi, P., Javadpour, F. and Sahimi, M., 2015. Multiscale and multiresolution modeling of shales and their flow and morphological properties. Scientific reports, 5(1), pp.1-11.
- Wang, Y., Teng, Q., He, X., Feng, J. and Zhang, T., 2019. CT-image of rock samples super resolution using 3D convolutional neural network.

Computers & Geosciences, 133, p.104314.

- Wildenschild, D., Vaz, C.M.P., Rivers, M.L., Rikard, D. and Christensen, B.S.B., 2002. Using X-ray computed tomography in hydrology: systems, resolutions, and limitations. Journal of Hydrology, 267(3-4), pp.285-297.
- Wildenschild, D. and Sheppard, A.P., 2013. X-ray imaging and analysis techniques for quantifying pore-scale structure and processes in subsurface porous medium systems. Advances in Water resources, 51, pp.217-246.
- You, N., Li, Y.E. and Cheng, A., 2021. 3D Carbonate Digital Rock Reconstruction Using Progressive Growing GAN. Journal of Geophysical Research: Solid Earth, 126(5), p.e2021JB021687.
- Zhu, J.Y., Park, T., Isola, P. and Efros, A.A., 2017. Unpaired image-to-image translation using cycle-consistent adversarial networks. In Proceedings of the IEEE international conference on computer vision (pp. 2223-2232).